optica

Exciting a chiral dipole moment in an achiral nanostructure: supplementary material

JÖRG S. EISMANN[1,2], MARTIN NEUGEBAUER[1,2], AND PETER BANZER[1,2,*]

[1] Max Planck Institute for the Science of Light, Staudtstr. 2, D-91058 Erlangen, Germany
[2] Institute of Optics, Information and Photonics, University Erlangen-Nuremberg, Staudtstr. 7/B2, D-91058 Erlangen, Germany
[*] Corresponding author: peter.banzer@mpl.mpg.de, http://www.mpl.mpg.de/

Published 3 August 2018

This document provides supplementary information to "Exciting a chiral dipole moment in an achiral nanostructure," https://doi.org/10.1364/OPTICA.5.000954, regarding the analysis of the FDTD simulations and the fit of the calculated far-fields to the polarization resolved far-field measurements. We also present additional simulation data showing how the average helicity and the chirality of the induced dipole moment is influenced by the excitation field.

1. ANALYSIS OF FDTD SIMULATIONS

For determining the scattered intensity displayed in Fig. 2 (d) of the main article, we performed two sets of simulations for each wavelength. The first simulation included only the air-glass interface without the particle on top (reference simulation). The second simulation includes the particle, exactly positioned on the optical axis. For the calculation of the incoming field of the spiral polarization beam, which is then introduced in the FDTD simulation, we use a numerical aperture (NA) of 0.9, adapted to our experimental situation. In the case without a particle, no light is entering the angular range above an NA of 0.9 in the far field in the lower half-space (glass). However, when the particle is included, we observe scattered light in this angular region above NA $= 0.9$. To obtain the graphs in Fig. 2 (d), we integrate over the intensity scattered into the angular region defined by NA $\in [0.92, 1.28]$ and divide it by the intensity integrated over the entire lower half space of the reference simulation. Using the same geometry like in the experiment is especially important for the comparison with the experimental results shown in Fig. 4 (a). In order to retrieve the relative phase $\varphi_{s,p}$ between the z-components of the electric and magnetic dipole moments [Fig. 2 (e)], we calculate the relative phase between the s- and p-polarized far-field components. Ideally, the relative phase between the dipole moments is preserved in their far-fields, as long as we consider the angular region below NA $= 1$ (corresponding to the angle of total internal reflection at the glass-air interface), where the Fresnel coefficients are real numbers and therefore do not introduce any additional relative phase between E_s and E_p. Therefore, we average the relative phase in the region defined by $0.92 \leq k_\perp/k_0 \leq 1.00$. Again, we want to prevent the influence of the transmitted excitation beam. The averaging is needed, since we still observe small fluctuations of the relative phase due to numerical imperfections.

2. POLARIZATION RESOLVED FAR FIELD FITTING

As it is mentioned in the main article, we performed a full polarization resolved far-field measurement for each wavelength, utilizing a rotatable achromatic quarter-wave plate and a fixed linear polarizer following the procedure explained in ref. [1]. With the data of all three far-field Stokes parameters it is possible to calculate the amplitudes of the transverse magnetic (E_p) and transverse electric (E_s) far fields, including their relative phase. This allows for a reliable fit of Eq. (2) of the main article to the experimental data. For our analysis, we consider the angular regime defined by a numerical aperture of NA $= [0.92, 1.28]$, because for our measured back focal plane images the influence of the directly transmitted beam is very strong below NA=0.9 (interference of the scattered light and the transmitted beam) and the highest collectable transverse k-vector of our oil-immersion-type objective is $k_\perp/k_0 = 1.3$. A slightly narrower angular range is used in order to avoid minor artifacts caused by diffraction at the pupils of the microscope objectives.

For the fit we start with an arbitrarily chosen combination of electric and magnetic z-dipoles and use a nonlinear regression in MATLAB to bring the calculated electric far-field [see equation (2) of the main article] as close as possible to the measurement result, where we use the complex amplitudes $A^\pm$ of the σ-dipoles [defined by equation (1) of the main article] as free parameters to maximize the overlap. When the fit has converged we calculate the field overlap between the experimentally determined electric fields and the theoretical fields corresponding to the final set of

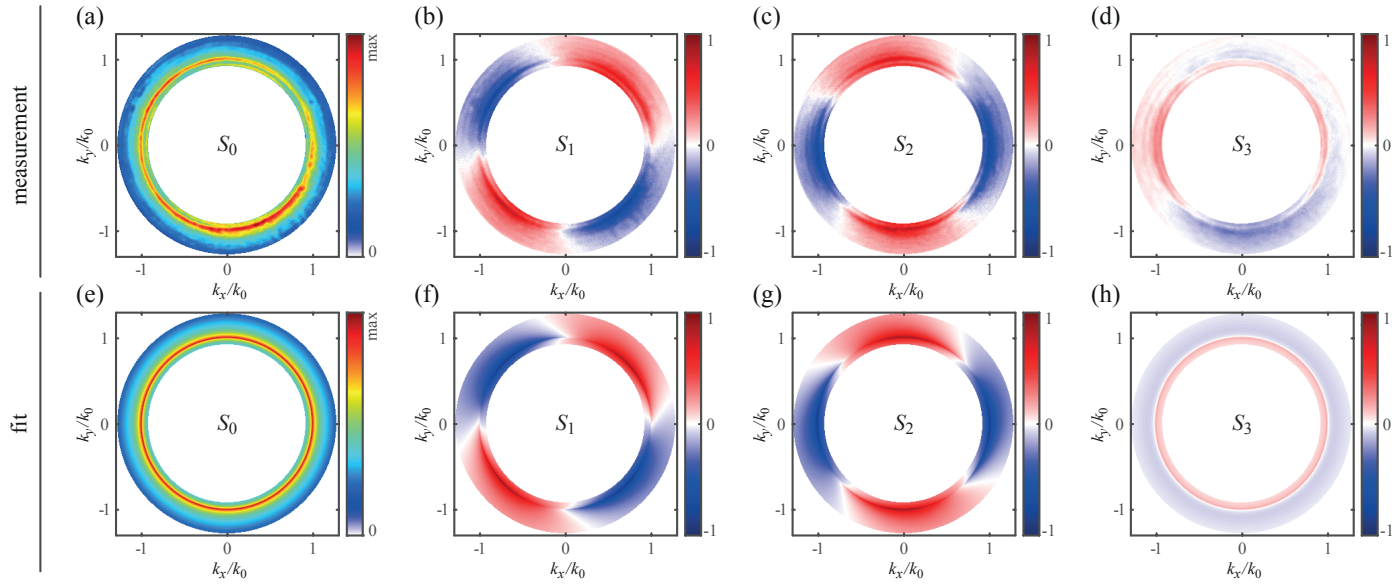

Fig. S1. Measured and fitted far-field Stokes parameter at 685 nm, depicted in an angular range defined by $0.92 < k_\perp/k_0 < 1.28$. (a)-(d) Polarization resolved back focal plane measurements. S_1, S_2, S_3 are normalized to the maximum value of S_0. (e)-(h) Theoretical far-fields calculated with Eq. (2) of the main article and the fitted parameters A^+ and A^-. Again we normalize S_1, S_2, S_3 to the maximum value of S_0.

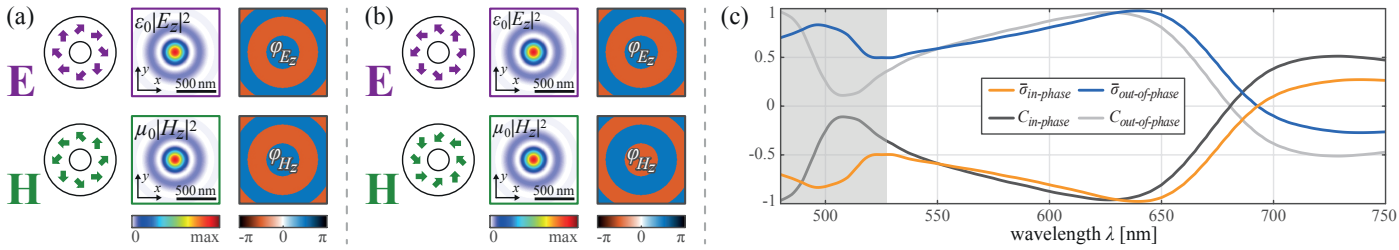

Fig. S2. FDTD simulations for different spiral polarization patterns. (a) and (b) illustrate the polarization distribution of two different incoming beams (in-phase and π out-of-phase superpositions of radially and azimuthally polarized beams) and the resulting longitudinal field components including phases in the focal plane. (c) The average helicity and chirality are depicted as orange and dark gray lines for the in-phase superposition [see also Fig. 4 (a) of the main article]. The blue and light gray lines represent the same parameters evaluated for the π out-of-phase superposition. The shaded gray area marks the spectral range where the magnetic quadrupole should be taken into account for a more precise calculation of the chirality of the dipole moments.

parameters utilizing the following equation:

$$\text{Field-overlap} = \frac{\iint \left| \begin{bmatrix} E_p \\ E_s \end{bmatrix}_{meas} \begin{bmatrix} E_p \\ E_s \end{bmatrix}^*_{fit} \right|^2 \mathrm{d}k_x \mathrm{d}k_y}{\iint \left| \begin{bmatrix} E_p \\ E_s \end{bmatrix}_{meas} \right|^2 \mathrm{d}k_x \mathrm{d}k_y \cdot \iint \left| \begin{bmatrix} E_p \\ E_s \end{bmatrix}_{fit} \right|^2 \mathrm{d}k_x \mathrm{d}k_y}. \quad \text{(S1)}$$

As an example, we show the complete set of measured far-field Stokes parameters at a wavelength of 685 nm in Fig. S1 (a)-(d). The third Stokes parameter is also shown in Fig. 4 (c) of the main article. In Fig. S1 (e)-(h) we display the theoretical counterparts, calculated with the fitted parameters. By comparing experiment and theory it becomes apparent why the field overlap is quite high, despite the asymmetry observable in the measured S_3 parameter.

3. SIMULATIONS FOR DIFFERENT INPUT BEAMS

In order to investigate the influence of the polarization distribution on the average helicity and chirality, we performed additional simulations for a spiral polarization beam featuring the opposite spiral polarization pattern. In contrast to the beam discussed and used in the main article (in-phase superposition of radially and azimuthally polarized beams), we now consider a π out-of-phase superposition. For comparison, a sketch of both incoming field distributions before focusing and the resulting focal filed distributions of the longitudinal fields are depicted in Figs. S2 (a) and (b). We show the simulation results for both input beams in Fig. S2 (c). As can be seen, the π out-of-phase superposition results in a sign flip of both the average helicity and the chirality.

REFERENCES

1. B. Schaefer, E. Collett, R. Smyth, D. Barrett, and B. Fraher, "Measuring the Stokes polarization parameters," Am. J. Phys. **75**, 163 (2007).